Biosensors and Bioelectronics 26 (2011) 2559–2565

Contents lists available at ScienceDirect

Biosensors and Bioelectronics

journal homepage: www.elsevier.com/locate/bios

# Xanthan/chitosan gold chip for metal enhanced protein biomarker detection

Patrick Domnanich, Dacimoneida Brito Peña, Claudia Preininger*

*AIT Austrian Institute of Technology GmbH, Health & Environment/Bioresources, 2444 Seibersdorf, Austria*

ARTICLE INFO

*Article history:*
Received 6 August 2010
Received in revised form 2 November 2010
Accepted 7 November 2010
Available online 14 December 2010

*Keywords:*
Metal enhanced protein chip
Melanoma biomarkers
Polyelectrolyte multilayers
Xanthan
Chitosan

ABSTRACT

Protein microarrays for disease diagnostics are required to accurately quantify analytes in the low pg/mL range. This task is hampered by weak signal strengths and too low detector sensitivity. Herein we present reflective gold chips coated with polyelectrolyte multilayers (PEMs) for signal enhancement in immunoassays for melanoma-relevant biomarkers. Among tested (semi)natural polysaccharides (xanthan, chitosan, carboxymethylcellulose, hyaluronic acid) PEMs composed of xanthan and chitosan performed best in terms of detection of low analyte concentrations (ED10), spot morphology, fluorescence background and variability (<10%). Fluorescence signals on gold slides with a 75 nm coating of seven crosslinked polyelectrolyte double layers were up to 50 times higher than on bare glass slides. In comparison to commercial substrates the signal to noise ratio is enhanced by up to factor 11. Furthermore sandwich assays for interleukins 6, 8, 10, tumour necrosis factor alpha (TNFα), vascular endothelial growth factor A (VEGF-A) and S100B show working ranges which cover significantly lower concentrations (up to 38-fold).

Not limited to above assays the presented substrates, which combine a biocompatible interface with metal-based signal amplification, are a valuable tool in a variety of biosensor applications.



## 1. Introduction

Protein microarrays are an emerging technology in clinical applications with diagnostic potential in many diseases such as melanoma (Domnanich et al., 2009). Though extremely promising accurate quantification of low abundance proteins in highly complex biological fluids like serum and plasma is still a major challenge in assay development. For instance cytokines, like interleukins 6, 8, 10 and TNFα, which are involved in many immunomodulatory processes and play a significant role in the development of melanoma, already act in pg/mL concentrations. These low analyte levels translate into small concentrations of labelled molecules and thus weak signals. If the collected signal intensity is comparable with the background intensity and the detector noise, it is difficult to extract reproducible information from the array.

This issue becomes even more acute if the assay is to be integrated into a portable diagnostic device. The high sensitive laser scanners with tuneable photomultiplier tube (PMT) cannot be used due to high costs, low scanning speeds and weight. Charge-coupled device (CCD) cameras offer a robust alternative for signal detection, yet in practical terms, their limit of detection is significantly higher than in PMT based scanners.

Low physical signal levels and poor detector sensitivity both hamper accurate quantification. Thus normal and moderately elevated levels of the biomarkers cannot be differentiated. To overcome this problem, samples may be preconcentrated and the incubation time may be prolonged. Unfortunately both strategies can also increase background fluorescence (Rifai et al., 2006). Moreover the available sample volume is often limited, and tedious, time-consuming tests have a low chance to find their way into clinical practice.

Alternatively signal amplification strategies and the use of surface enhancing matrices, that increase biomolecule immobilization capacity and promote protein stability, can help to attain the required assay sensitivities.

Amplification of the optical signal has been achieved with advanced labels including quantum dots, fluorescent nanoparticles and fluorescent proteins or by applying enzymatic and chemical reactions. Furthermore, metallic surfaces and nanometallic objects such as noble metal nanoparticles and colloids, silver nanostructures and metal island films were exploited for signal enhancement. These techniques are based on a concept termed metal-enhanced fluorescence and make use of reflective and surface plasmonic effects thereby changing the light emission properties of the nearby fluorophores (Ray et al., 2010; Schuller et al., 2010).

By contrast, improved assay performance as a result of superior surface materials used for protein immobilization was obtained by applying porous supports and surface enlarging nanostructures, dendrimers, hydrogels and polyelectrolyte multilayers (PEMs) (Lee

* Corresponding author. Tel.: +43 50550 3527; fax: +43 050 550 3666.
*E-mail address:* Claudia.Preininger@ait.ac.at (C. Preininger).

0956-5663/$ – see front matter © 2010 Elsevier B.V. All rights reserved.
doi:10.1016/j.bios.2010.11.006

et al., 2007). PEMs are thin films constructed by alternative adsorption of oppositely charged polyelectrolytes from their aqueous solutions using a layer-by-layer (LbL) technique. Due to multiple charge neutralisation interactions, PEMs are highly stable. Moreover the method is capable of varying film composition and provides enormous design flexibility. Thus it is not surprising that PEMs receive increasing attention in medical as well as in biotechnological applications.

In this study, we combine both physical signal amplification and a biocompatible PEM hydrogel for protein immobilization. We build up an assembly of PEMs on gold substrates and optimize conditions for metal enhanced fluorescence. Slides are printed with arrays of antibodies against several cytokines and melanoma biomarkers: IL6, IL8, IL10, TNFα, S100B and VEGF. We evaluate the respective assays in 10% human serum and demonstrate the superior performance of the gold PEM substrates in comparison to commercial slides.

## 2. Materials and methods

### 2.1. Materials and reagents

ARChips Epoxy are proprietary slides developed at AIT. BioGold coated substrates and poly-L-lysine slides were from Erie Scientific Company. Histobond slides, positively charged glass slides, were from Marienfeld. Nexterion HiSens Slides E (reflective slides) for high-sensitive detection are from Schott. Phosphate buffered saline (PBS) was purchased from Gibco. Polyoxyethylene–sorbitan monolaurate (Tween-20), bovine serum albumin (BSA), sodium chloride, sodium deoxycholate, N-(3-dimethylaminopropyl)-N′-ethylcarbodiimide (EDC), N-hydroxysuccinimide (NHS), protein G, medium molecular weight chitosan (>75% deacetylation, viscosity 200–800 cps at 1%), xanthan gum from *Xanthomonas campestris* (Brookfield viscosity 800–1200 cps at 1%) and sodium carboxymethyl cellulose (average Mw ~250,000) were purchased from Sigma. Sodium hyaluronate from *Streptococcus pyrogenes* (Mw $5.0 \times 10^5$–$1.2 \times 10^6$) was from Merck.

Anti-S100 protein (MAb 8B10), biotinylated anti-S100 protein (MAb 6G1), human S100 protein, biotinylated anti-human TNFα (F6C5) and CRP-free serum were purchased from HyTest (Finland). Monoclonal anti-VEGF (Clone 26503) and biotinylated anti-VEGF antibody (BAF293) were from R&D Systems. Anti-human TNFα (B-F7) and recombinant human TNFα were from Exbio Praha. Anti-IL8 antibody (H8A5), recombinant human IL8 and biotinylated anti-IL8 antibody (E8N1) were from Biolegend.

Recombinant human VEGF-A was from Invitrogen Corporation. Recombinant human IL6, IL10, biotin-conjugated anti-human IL6 (MQ2-39C3) and anti-IL10 (JES3-12G8) proteins as well as anti-human IL6 (MQ2-13A5) and anti-human IL10 (JES3-9D7) antibodies were from eBioscience. Fluorolink Cy5 labelled streptavidin was from Amersham Biosciences UK Limited.

### 2.2. Substrate preparation

Substrates for PEM microarray fabrication were positively charged glass slides and gold slides. PEMs were deposited using a KSV dip coater model D: First slides were incubated in 1 mg/mL of negatively charged polyelectrolyte in 150 mM NaCl (adjusted to pH 5 with acetic acid) for 900 s. The negatively charged polyelectrolyte was xanthan, carboxymethylcellulose or hyaluronic acid. Afterwards substrates were washed three times in 150 mM NaCl for 360 s. Next, slides were incubated alternating in 1 mg/mL chitosan, 150 mM NaCl (pH 5) and 1 mg/mL of the negatively charged polyelectrolyte, 150 mM NaCl (pH 5) for 360 s each. Each polyelectrolyte incubation step was followed by three washing steps in 150 mM NaCl for 360 s. The process was repeated until the desired number of polyelectrolyte bilayers was deposited (Fig. 1a). For crosslinking slides were treated in NHS (20 mM)/EDC (10 mM) for 2 h and subsequently washed in water.

### 2.3. Probe arraying and blocking

0.4 mg/mL anti-IL6, 0.4 mg/mL anti-IL10, 0.4 mg/mL anti-IL8, 1 mg/mL anti-TNFα, 0.5 mg/mL anti-VEGF-A, 1 mg/mL anti-S100B and 1 mg/mL protein G in print buffer (1× PBS, pH 7.2, 0.01% sodium deoxycholate) were arrayed on PEM modified substrates (Fig. 1b), epoxy slides, poly-L-lysine slides and reflective slides at 70% relative humidity using the contact spotter OmniGrid from GeneMachines (2 pins SMP3). Spot-to-spot distance was 400 μm and array-to-array distance was 8950 μm. All probes were immobilized in triplicate and 10 identical arrays were spotted per slide.

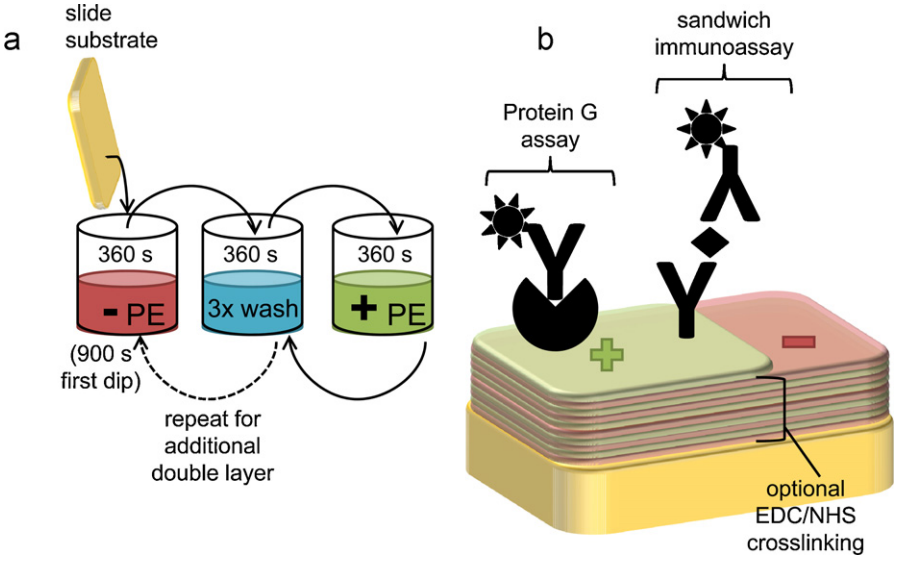


**Fig. 1.** Fabrication and use of polyelectrolyte multilayer slides. (a) PEMs are assembled on substrates by sequential incubations in negatively (− PE) and positively charged polyelectrolytes (+ PE). (b) PEM substrates serve as platforms for electrostatic binding of proteins like protein G or anti-IL10. The polyelectrolyte layers might be additionally crosslinked with EDC/NHS.

After spotting slides were kept in a humid chamber at 4 °C for a minimum of three days to ensure complete probe immobilization.

Before the experiment EDC/NHS activated substrates were treated in 1 M ethanolamine (pH 9) for 10 min to inactivate residual NHS esters. Epoxy slides were blocked for 30 min in 1× PBS (pH 7.2)/0.1% Tween-20 to remove any unbound receptors. Blocking of the other substrates was performed in 1× PBS (pH 7.2)/1% BSA/0.1% Tween-20 for 30 min at room temperature (RT). Afterwards slides were washed twice in 1× PBS (pH 7.2) and dry-centrifuged for 4 min (900 rpm).

### 2.4. Chip processing

All incubation steps were done at RT on The Belly Dancer (Stovall, Greensboro, NC, USA). Slides were processed applying the Fast Frame system (Whatman) with 16 well incubation chambers.

For the protein G assay substrates were incubated in 1 μg/mL Dy647-conjugated anti-procalcitonine antibody in assay buffer (0.1 M Tris, pH 7.4, 10 mM $CaCl_2$, 100 mM NaCl) for 45 min. Slides were washed 2 times in 1× PBS (pH 7.2)/0.1% Tween-20, 2 times in 1× PBS (pH 7.2) and dry-centrifuged for 4 min (900 rpm).

For the sandwich immunoassays antigen standards were prepared by serial dilution of an antigen mix (IL6, IL8, IL10, VEGF-A, S100B, TNFα) in a matrix of CRP-free HyTest serum diluted 1:10 with assay buffer.

Bound monoclonal capture antibodies were incubated with antigen standards for 120 min. Next, wells were washed three times with 1× PBS (pH 7.2)/0.1% Tween-20 and incubated with 1 μg/mL of each of the biotin-labelled antibodies anti-IL6, anti-IL10, anti-IL8, anti-TNFα, anti-VEGF-A and anti-S100B in assay buffer for 45 min.

After washing 3 times with PBS (pH 7.2)/0.1% Tween-20 wells were treated with 2 μg/mL Cy5 labelled streptavidin in assay buffer for 45 min. Finally slides were washed 2 times in 1× PBS (pH 7.2)/0.1% Tween-20, 2 times in 1× PBS (pH 7.2) and dry-centrifuged for 4 min (900 rpm).

### 2.5. Fluorescence detection and data analysis

Slides were stored in the dark till scanning. Fluorescence measurements ($\lambda_{ex}$ = 635 nm, $\lambda_{em}$ = 670 nm) were taken using a Genepix 4000B non-confocal scanner (Axon Instruments). For data comparison, the scanner photomultiplier tube gain was kept constant throughout scans. Reported fluorescence signals are background corrected and calculated as mean values from at least 6 replicate spots. Calibration curves were set up using the five parameter logistic model (stats package of the statistic program R). ED*x* value is the estimated effective analyte concentration for the signal response level of *x*%. Moreover the slope *k* at the ED50 was calculated. The coefficient of variation (CV% = SD/mean × 100) was a measure for data reproducibility. Signal-to-noise ratios were computed for each data point by dividing the mean fluorescence intensity of the spot after background subtraction with the mean fluorescence intensity of the same spots in assays without added analyte.

### 2.6. Contact angle measurements

Contact angle measurements were performed with a CAM101 (KSV Instruments). Reported values were calculated from at least 6 replicate measurements.

### 2.7. Measurement of polyelectrolyte coating thickness

PEM thickness measurements were carried out at scratches with a Nanowizard II (JPK Instruments) atomic force microscope (AFM) with cantilever CSC38/AIBS (MikroMasch) in contact mode. Reported values were calculated from at least five measurements taken at different positions.

## 3. Results and discussion

### 3.1. Evaluation of polysaccharide PEM systems for protein immobilization

PEMs have proven to be favourable matrices in protein and enzyme technology as many immobilized proteins were reported to retain their activity for prolonged times. This effect was frequently attributed to the gel-like environment which keeps proteins hydrated and in a native conformation (Zhou and Zhou, 2006).

Typical polyelectrolytes reported for protein microarray fabrication are poly(vinylsulfonate), poly(styrenesulfonate) (PSS), poly(acrylate), poly(allylamine) and poly(ethyleneimine) (Dai et al., 2005; Shim et al., 2007; Spillman et al., 2008; Sung et al., 2009; Zhou and Zhou, 2006). Unlike those macromolecules we employ (semi)natural polysaccharides for on-chip multilayer assembly: chitosan (CS) as positively charged building block, and either hyaluronic acid (HA), carboxymethylcellulose (CMC) or xanthan (XA) as anionic PEM component.

PEM assemblies made from these compounds were evaluated as protein microarray platforms. In order to avoid messing up with thickness dependent gold enhancement effect PEM architectures of five double layers were built on positively charged glass substrates (Fig. 1b) rather than on gold substrates. Evaluation criteria were low autofluorescence at the excitation wavelength ($\lambda_{ex}$ = 635 nm), high assay sensitivity for protein G in a direct fluorescence assay, uniform spot morphology, low fluorescence background and good reproducibility.

The autofluorescence of HA/CS, CMC/CS and XA/CS assemblies was comparable and similar to that of a bare glass slide. Thus the PE layers do not significantly contribute to the chip's autofluorescence. In order to evaluate assay performance we spotted protein G (isoelectric point of 4.2) and incubated with fluorescently labelled antibody (Table 1). While signals were similar for both $[HA/CS]_5$ and $[XA/CS]_5$, signals obtained on the $[CMC/CS]_5$ assembly were dramatically reduced (by about 85%). In contrast to spots on $[CMC/CS]_5$ which feature a doughnut morphology, spots on both $[HA/CS]_5$ and $[XA/CS]_5$ are homogeneous and regular without comet effects. Yet the interspot-variability on $[XA/CS]_5$ only amounts to 4% in comparison to 13% on $[HA/CS]_5$ (Table 1). The highest variability is found for $[CMC/CS]_5$. The differences in signal intensity and spot morphology can be attributed to the influence of the polyanionic compound: its charge density and chemical topology govern the thickness and structure of the terminally deposited chitosan layer and thus the performance of the immobilized array. Also it has been reported

**Table 1**
Performance characteristics of different PEMs on glass slides. CV calculated from 30 replicate spots.

| Coating | Signal (a.u.) | CV (%) | Background (a.u.) | Spot morphology |
|---|---|---|---|---|
| $[CMC/CS]_5$ | 5489 | 23 | 68 |  |
| $[XA/CS]_5$ | 35251 | 4 | 82 |  |
| $[HA/CS]_5$ | 35628 | 13 | 97 |  |
| $[HA/CS]_4HA$ | 29784 | 18 | 129 |  |

**Table 2**
PEM thickness and figures of merit of IL10 assay standard curves on gold slides with 1, 3, 5, 7, 9 and 12 [XA/CS] double layers.

| PEM | Thickness (nm) | ED10 (pg/mL) | ED90 (pg/mL) | ED50 (pg/mL) | Slope | Mean CV (%) | Dynamic range |
|---|---|---|---|---|---|---|---|
| $[XA/CS]_1$ | <2 | 167 | 46,718 | 2790 | 0.40 | 9 | 280 |
| $[XA/CS]_3$ | $2 \pm 2$ | 251 | 120,342 | 5491 | 0.70 | 9 | 480 |
| $[XA/CS]_5$ | $31 \pm 1$ | 18 | 29,002 | 726 | 0.64 | 28 | 1595 |
| $[XA/CS]_7$ | $74 \pm 3$ | 5 | 1201 | 166 | 0.83 | 5 | 141 |
| $[XA/CS]_9$ | $141 \pm 11$ | 100 | 30,600 | 1746 | 0.83 | 12 | 307 |
| $[XA/CS]_{12}$ | $247 \pm 21$ | 24 | 7588 | 431 | 0.73 | 11 | 310 |

(Yoo et al., 1998) that polyelectrolyte layer interpenetration leads to modification of surface properties by an underlying layer.

Termination of the assemblies by a layer of chitosan, instead of the anionic polysaccharide, contributes to a lower unspecific background as can be seen clearly from the comparison between the chitosan and the hyaluronic acid terminated systems $[HA/CS]_5$ and $[HA/CS]_4HA$ (Table 1). This phenomenon may be explained by a more efficient blocking step on the chitosan surface. At physiological pH, the negatively charged blocking agent BSA ($pI \approx 5.5$) (Chang et al., 2005) will adsorb on polycationic chitosan, whereas adsorption on the polyanion is impeded by electrostatic repulsion.

Changes in the background level also occur among chitosan terminated PEMs (Table 1). The lowest background is found for $[CMC/CS]_5$, whereas background fluorescence of $[XA/CS]_5$ is slightly decreased in comparison to $[HA/CS]_5$.

Thus owing to the low background, excellent spot morphology and reproducibility, as well as the high signal strengths, the $[XA/CS]_5$ system was chosen as PEM support.

### 3.2. The xanthan/chitosan system

To create stable PEMs we investigated the effect of matrix crosslinking and studied the assembly of the system on gold substrates as characterized by contact angle and layer thickness.

#### 3.2.1. Crosslinking

In this study the PEM film serves as a spacer between the gold surface and the fluorophores. When transferring the PEM assembly from the glass support to a gold substrate (see Section 3.2.2) controlled layer thickness and uniformity become important as metal enhanced fluorescence strongly depends on the distance between the labelled antibodies and the gold layer. However the assay procedure, which involves both incubation steps at different ionic strengths and mechanical strains, stresses the PEM.

Unlike other polyelectrolyte systems XA/CS multilayers are insensitive to changes in ionic strength and do not swell due to the high chain stiffness of xanthan (Maurstad et al., 2005). In order to further strengthen the film the layer was stabilized by EDC/NHS crosslinking which couples the activated carboxylate groups of xanthan to the amino groups of chitosan. We found that the crosslinked XA/CS PEM exhibits a dramatically smoother and more homogeneous surface than the native one: AFM thickness measurements for crosslinked films did not vary by more than 20%. In contrast, thickness measurements for native XA/CS PEMs varied by about 700%, reflecting a very rugged surface. Thus crosslinking was chosen to provide a strengthened surface of homogeneous thickness.

#### 3.2.2. PEM assembly on gold chips

To achieve signal amplification in an assay set-up, the XA/CS PEM was assembled on a reflective metal substrate. Gold substrates were chosen, as gold is both stable at physiological conditions and insensitive to humidity and prolonged storage.

PEMs can be either deposited directly onto gold substrates (Spillman et al., 2008) or onto a priming monolayer of self-assembled carboxythiol (Caruso et al., 1997). The first scenario is very attractive as the gold surface can be used without any special pre-treatment. However to ensure stable initiation of multilayer growth, this approach demands good adherence of the PEM components to the uncharged bare gold substrates. To test for adsorption of XA and CS to gold, substrates were immersed in either solution of the polyelectrolyte and rinsed in wash solution. The water contact angle, a very sensitive indicator for surface modifications, was recorded. Clearly, both hydrophilic polymers CS and XA adsorb to the gold surface. This is reflected by a significant decrease in the contact angle of CS on gold ($51.8 \pm 4.6^\circ$) and XA on gold ($74.8 \pm 2.1^\circ$) as compared to bare gold slides ($83.3 \pm 1.9^\circ$). Therefore both polyelectrolytes can contribute to tether the PEM assembly to the gold surface and no mediating layer is needed for adhesion. PEMs were stable during chip processing (Section 3.4) as indicated by well defined fluorescence spots (see Fig. 4a).

#### 3.2.3. Thickness of the PEM assembly

Thickness of the XA/CS system increases strongly with the number of deposited bilayers (Table 2). After a short lag-phase of about 3 polyelectrolyte bilayers, a stable growth regimen dominated by the multilayer charge density is reached. These growth characteristics apply to both PEM assemblies on Au and glass slides.

While 3 bilayers build up to about 5 nm thick hydrogel layer, 12 bilayers amount to a 250 nm thick assembly. Such a growth regimen is typical for so-called exponentially growing PEMs. In contrast to linearly growing films, which feature heights between 50 and 100 nm after the deposition of 20 bilayers, exponentially growing films show thicknesses between 0.1 and 10 μm. This behaviour facilitates the built-up of films of substantial thickness after only several polyelectrolyte deposition cycles.

### 3.3. Effect of metal enhanced fluorescence

AFM thickness measurements reveal spacer layers on gold slides ranging from several nm (1 bilayer of [XA/CS]) up to 250 nm (12 bilayers). Using these slides signal amplification was studied in a sandwich immunoassay for IL10 at an antigen concentration of 780 pg/mL, which is within the linear assay range. Control experiments with the same polyelectrolyte assemblies on glass slides were carried out (Fig. 2). While the control experiments showed a very weak dependence of signal strengths on PEM thickness (number of deposited bilayers), a significant difference is seen for gold carrier substrates: signal on gold substrates is significantly smaller than on glass supports for 1 and 3 polyelectrolyte bilayers. This phenomenon can be explained by quenching of the dye molecules in the vicinity of the gold surface, as the distance amounts only to several nm. However the situation changes dramatically as the PEM assembly continues to grow. At 5 double layers (31 nm thickness) signal intensity on gold is about 6 times higher than on the glass control. On a 7 double layer PEM (74 nm) the amplification factor raises to 13. Then, at 9 double layers (141 nm), amplification dramatically breaks down and increases again at 12 bilayers. Thus a fluorescence signal maximum is found at 7 XA/CS bilayers. The

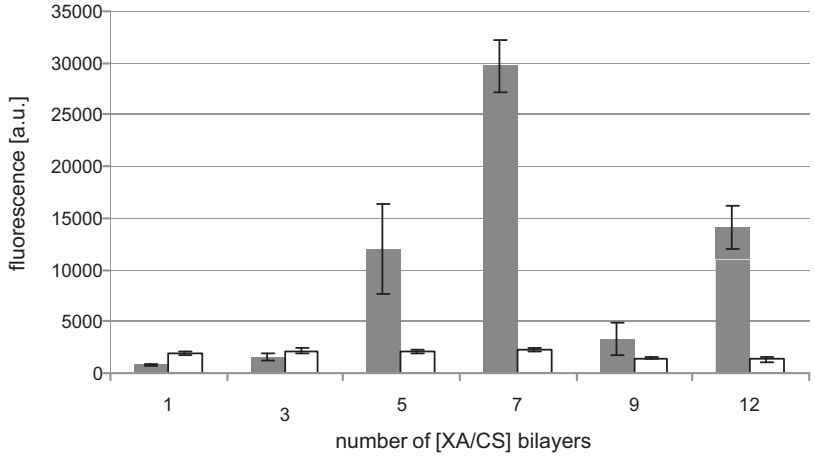


**Fig. 2.** The number of deposited [XA/CS] polyelectrolyte bilayers affects IL10 sandwich immunoassay signal strengths. PEM coated substrates were gold (grey) and glass (white).

amplification factor amounts to about 50 and 13, as compared to the untreated glass slide and glass slides coated with 7 bilayers of XA/CS respectively. This illustrates that both the protein-friendly gel environment of the polyelectrolyte and the gold substrate contribute to fluorescence enhancement.

The metal substrate associated amplification phenomenon can grossly be explained by the fact that emitted fluorescence light, which is normally scattered and lost through the glass substrate, is reflected back to the detector by the gold mirror. However, as can be seen from the data, the amplification factor is not constant but varies periodically with the thickness of the transparent layer between the fluorophore and the underlying reflecting surface. The observed oscillating trend was confirmed with different batches of polyelectrolyte slides which were spotted and processed on different days. Additionally the phenomenon was previously reported on reflective silicon wavers coated with $SiO_2$ layers of defined thickness (Cretich et al., 2009; Lambacher and Fromherz, 1996; Moiseev et al., 2004). The oscillating signal amplification is thought to arise from interference phenomena: both incident and emitted light independently interfere with their reflection from the mirror. Depending on the distance between dye and metal surface either constructive wave interference leads to amplification maxima or destructive interference results in attenuation of the signal. Thereby enhanced signal intensities are associated with shortened excitation lifetimes and increased quantum yields of the fluorophores (Ray et al., 2010).

Qualitatively the observed oscillating trend with strongest amplification at a coating thickness of about 75 nm perfectly corresponds to the theoretical calculations by Bras et al. (2004). They investigate a dye layer on a $Si/SiO_2$ system and predict the first and strongest amplification maximum for Cy5 at a $SiO_2$ thickness of about 100 nm. A further maximum is at 320 nm, whereas attenuation is maximal at 0 and 210 nm. The quantitative divergence between the $SiO_2$ system and the polyelectrolyte system in this study has two reasons: firstly, the distance between amplification maxima in the XA/CS system is smaller. This is, because the phase-shift leading to interference is caused by the length of the optical light path through the transparent spacer layer. Therefore spacer layers with higher refractive index result in amplification patterns with apparent lower periodicity. This is reasonable, as many natural polysaccharide films have refractive indices higher than that of fused silica, $SiO_2$ ($n = 1.46$ at 650 nm (Malitson, 1965)), e.g. chitosan ($n = 1.53$ (Nosal et al., 2005)). Secondly, in our approach, the dye molecule is not directly situated at the air–PEM interface but located on top of the IL10 immunosandwich. This results in an additional distance of several nm.

### 3.4. Gold enhanced assays for melanoma-relevant protein biomarkers

Having observed increasing signal strengths on gold substrates with up to 7 double layers of XA/CS, we studied the amplification effect on whole calibration curves. Investigated parameters were the working range defined as 10–90% of the signal range (ED10 and ED90), ED50, the slope of the curves and the variability (mean CV). Furthermore the dynamic range was estimated. It was calculated as the ratio ED90/ED10. ED10 and ED90 are the effective analyte concentrations giving 10% and 90% of the assay's maximal possible fluorescence signal response. The effect of a growing number of XA/CS layers on IL10 calibration curves is shown in Fig. 3. Figures of merits are sampled in Table 2. When increasing the number of deposited PEM double layers from 1 to 3, the working range broadens due to the strong rise of the upper limit of the working range (ED90). When the number of double layers further grows to 5 and 7, the working range successively downshifts to lower concentration ranges. The downshift of the ED50, the midpoint of the

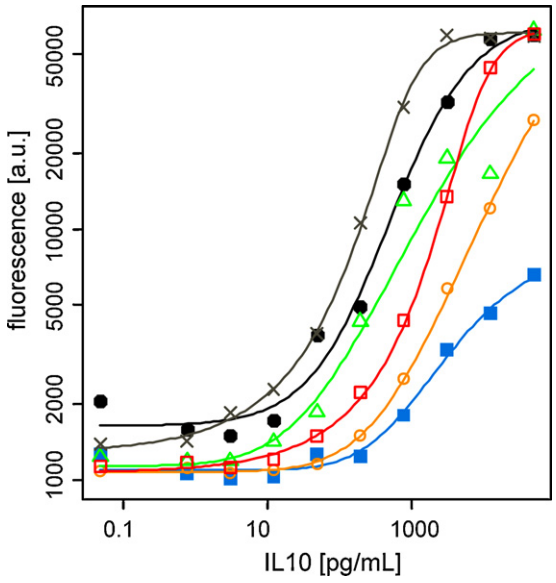


**Fig. 3.** Amplification affects working range of calibration curves. IL10 sandwich immunoassay was performed on gold slides coated with increasing number of [XA/CS] bilayers: 1 bilayer (■), 3 (○), 5 (△), 7 (×), 9 (□), and 12 (●) bilayers. Mean CVs are given in Table 2.

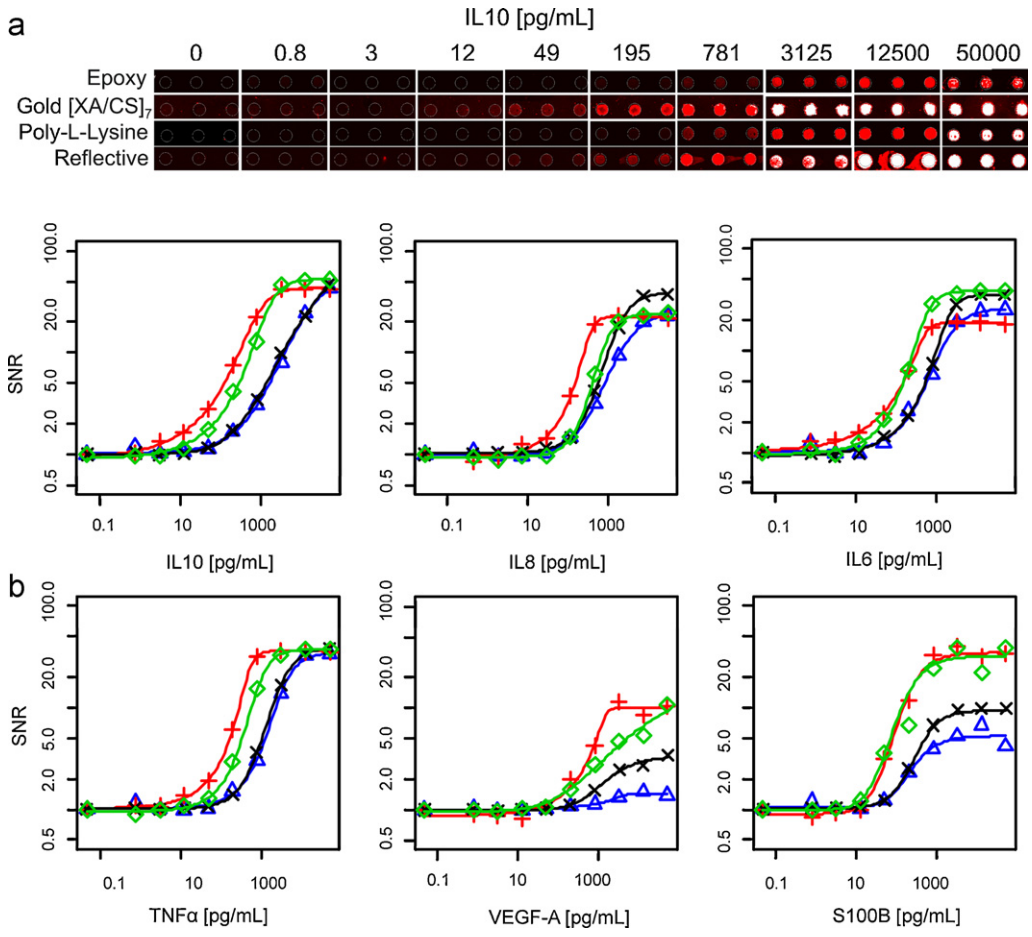


**Fig. 4.** Comparison of PEM substrates to commercial slides. (a) Spots of IL10 sandwich immunoassay on different substrates. (b) Standard curves for melanoma-relevant immunoassays expressed as SNR on gold $[XA/CS]_7$ (+), commercial reflective high sensitivity (◊), epoxy (△) and poly-L-lysine slides (×).

working range, from 5491 pg/mL for 3 double layers to 166 pg/mL for 7 double layers clearly illustrates that quantifications at lower concentrations become possible. Opposed to this trend, at 9 double layers the ED50 range strongly shifts up to higher concentrations. Finally at 12 double layers the ED50 is again at lower concentrations (431 pg/mL). The same trend is observed for the ED10 values which mark the beginning of the working range. This oscillating behaviour is in complete agreement with the oscillating signal intensities obtained in Section 3.3. In summary slides coated with 7 double layers of XA/CS exhibit lowest ED10 and ED50. The standard curves' slope rises significantly when increasing the number of polyelectrolyte bilayers from 1 to 3 and subsequently stagnates at a value around 0.7.

Reproducibility, expressed by a low mean CV, is optimal at 7 double layers.

The dynamic range of the IL10 assay is around 300 for 1, 9 and 12 double layers. It is extended for 3 double layers and the highest value is reached for 5 double layers. The dynamic range for $[XA/CS]_7$ is smaller because the signal intensities generated on this substrate are so high, that the detector is already saturated at an IL10 concentration of about 1000 pg/mL. Lowering the detector sensitivity would thus increase the $[XA/CS]_7$ dynamic range. However as the aim of the slide development is accurate quantification of low analyte concentrations we put the emphasis on low ED10 and ED50, high slope and a low CV. Owing to the excellent performance in these parameters gold slides coated with 7 double layers of XA/CS were used for further comparisons.

### 3.4.1. Commercial slides

Gold $[XA/CS]_7$ substrates were compared with commercial epoxy and poly-L-lysine slides as well as with commercial reflective slides. Fluorescence images shown in Fig. 4a illustrate that the substrates exhibit largely different signal strengths: For example at 195 pg/mL IL10 signals on the polyelectrolyte slides are about 6 times as high as on epoxy and poly-lysine surfaces and about twice the strength as on the reflective slides. Consequently signal saturation (white spots) occurs for gold $[XA/CS]_7$ already at 3125 pg/mL IL10, whereas reflective and poly-lysine slides are fully saturated at only 12,500 pg/mL and 50,000 pg/mL respectively. While commercial reflective slides exhibit excessive smearing at high analyte concentrations, polyelectrolyte surfaces produce homogenous, consistent spots throughout all tested concentrations. Also slides have very different sensitivities: the PEM slides are the only tested substrates that show significant spot intensities at 12 pg/mL IL10.

In order to compare the assay performance of these very different chip surfaces we calculated the signal-to-noise ratios (SNRs) for each spot and plotted SNR as a function of the analyte concentration. Calibration curves for the markers IL10, IL8, IL6, TNFα, S100B and VEGF-A (Fig. 4b) reveal that SNRs for gold $[XA/CS]_7$ are excellent even at extremely low analyte concentrations. In comparison to the other slides the increases in SNR amount up to factor 11 (between PEM slides and epoxy for analyte TNFα). Stagnation of the SNRs at very high concentrations is due to saturation effects.

Our primary aim is to use chips to quantify proteins at very low concentrations. One prerequisite for accurate quantifications

is high reproducibility. Surprisingly, reproducibility is remarkably similar for all slide types, ranging from a CV of 6 ± 2% for the poly-lysine slides to 8 ± 4% for the epoxy slides. Likewise the slopes of the curves on the different substrates are comparable for many of the analytes. Yet clear differences in the working range are discernible: Epoxy and poly-lysine surfaces feature rather similar standard curves (Fig. 4b) and working ranges (supplementary information, Table S1). In comparison to poly-lysine slides standard curves of XA/CS and reflective slides experience a left-shift to lower concentrations. For the XA/CS slides this shift clearly depends on the analyte and varies between factor 3 for VEGF-A (determined as the ratio between respective ED50 values) and factor 23 for IL10. The lower limit of the working range even decreases between factor 3 for S100 and factor 38 for IL10.

Apart from the S100 immunoassay, where gold $[XA/CS]_7$ and reflective slides produce similar curves, XA/CS slides cover working ranges at lower analyte concentrations than the reflective slides: curves are left-shifted between factor 1.4 (IL6) and 3 (IL8).

## 4. Conclusion

Among three tested (semi)natural polysaccharide PEMs we chose the xanthan/chitosan system for the assembly of coatings on gold substrates. Thorough optimization of the layer thickness and homogeneity led to significant fluorescence signal enhancements on gold xanthan/chitosan slides in comparison to PEM coated glass substrates and to even larger gains, up to factor 50, in respect to bare glass slides. This finding illustrates that both the protein-friendly gel environment of the polyelectrolyte assembly and the metal enhancement of fluorescence via the gold substrates contribute to the amplification process.

Comparing the performance of melanoma-relevant sandwich immunoassays on gold PEM slides to commercial substrates in 10% human serum we found

- up to 6-fold increased signal strengths;
- superior signal to noise ratios (up to 11-fold);
- a left-shift of the working range enabling quantifications at significantly lower concentrations.

Furthermore the PEM layer, which is deposited by a simple aqueous LbL dipping technique, has the potential to be applied to gold – and (possibly) other reflective metal surfaces – of virtually any geometry. Involving biocompatible materials this amplification technique is envisioned to be a valuable tool in a variety of biosensor applications.

## Acknowledgements

The authors thank the Austrian Science Foundation FWF and the Spanish Ministry of Education for financial support through the Translational-Research (L415-N19) and the ARGO programme.

## Appendix A. Supplementary data

Supplementary data associated with this article can be found, in the online version, at doi:10.1016/j.bios.2010.11.006.

## References

Bras, M., Dugas, V., Bessueille, F., Cloarec, J.P., Martin, J.R., Cabrera, M., Chauvet, J.P., Souteyrand, E., Garrigues, M., 2004. Biosensors and Bioelectronics 20 (4), 797–806.
Caruso, F., Niikura, K., Furlong, D.N., Okahata, Y., 1997. Langmuir 13 (13), 3427–3433.
Chang, W.W.P., Hobson, C., Bomberger, D.C., Schneider, L.V., 2005. Electrophoresis 26 (11), 2179–2186.
Cretich, M., di Carlo, G., Longhi, R., Gotti, C., Spinella, N., Coffa, S., Galati, C., Renna, L., Chiari, M., 2009. Analytical Chemistry 81 (13), 5197–5203.
Dai, J., Baker, G.L., Bruening, M.L., 2005. Analytical Chemistry 78 (1), 135–140.
Domnanich, P., Sauer, U., Pultar, J., Preininger, C., 2009. Sensors and Actuators B: Chemical 139 (1), 2–8.
Lambacher, A., Fromherz, P., 1996. Applied Physics A: Materials Science and Processing 63 (3), 207–216.
Lee, J.-H., Shim, H.-W., Choi, H.-S., Son, Y.-A., Lee, C.-S., 2007. Journal of Physics and Chemistry of Solids 69 (5–6), 1581–1584.
Malitson, I.H., 1965. Journal of the Optical Society of America 55 (10), 1205–1208.
Maurstad, G., Bausch, A.R., Sikorski, P., Stokke, B.T., 2005. Macromolecular Symposia 227 (1), 161–172.
Moiseev, L., Cantor, C.R., Aksun, M.I., Dogan, M., Goldberg, B.B., Swan, A.K., Unlu, M.S., 2004. Journal of Applied Physics 96 (9), 5311–5315.
Nosal, W.H., Thompson, D.W., Yan, L., Sarkar, S., Subramanian, A., Woollam, J.A., 2005. Colloids and Surfaces B: Biointerfaces 43 (3–4), 131–137.
Ray, K., Chowdhury, M., Zhang, J., Fu, Y., Szmacinski, H., Nowaczyk, K., Lakowicz, J., 2010. In: Rao, G. (Ed.), Optical Sensor Systems in Biotechnology. Springer, Berlin/Heidelberg, pp. 29–72.
Rifai, N., Gillette, M.A., Carr, S.A., 2006. Nature Biotechnology 24 (8), 971–983.
Schuller, J.A., Barnard, E.S., Cai, W., Jun, Y.C., White, J.S., Brongersma, M.L., 2010. Nature Materials 9 (3), 193–204.
Shim, H.-W., Lee, J.-H., Hwang, T.-S., Rhee, Y.W., Bae, Y.M., Choi, J.S., Han, J., Lee, C.-S., 2007. Biosensors and Bioelectronics 22 (12), 3188–3195.
Spillman, S.D., McEvoy, H.M., MacCraith, B.D., 2008. Langmuir 25 (3), 1403–1411.
Sung, W.-C., Chen, H.-H., Makamba, H., Chen, S.-H., 2009. Analytical Chemistry 81 (19), 7967–7973.
Yoo, D., Shiratori, S.S., Rubner, M.F., 1998. Macromolecules 31 (13), 4309–4318.
Zhou, X., Zhou, J., 2006. Proteomics 6 (5), 1415–1426.